PHOTOCATALYTIC DEGRADATION OF RHODAMINE B OVER PERSULFATE-ACTIVATED $(BIO)_2CO_3$@$ZNCO_2O_4$ UNDER VISIBLE LIGHT

NGUYEN THI MAI THO*; NGUYEN QUOC THANG
Faculty of Chemical Engineering, Industrial University of Ho Chi Minh City, Ho Chi Minh, Vietnam.
** Corresponding author: nguyenthimaitho@iuh.edu.vn*
DOIs: https://www.doi.org/10.46242/jstiuh.v81i3.6007

Abstract. In this study, a heterojunction photocatalyst, $(BiO)_2CO_3$@$ZnCo_2O_4$, was synthesised via a co-precipitation method. The physicochemical properties of the as-synthesised were characterised by XRD, FT-IR, SEM, TEM, and UV–Vis DRS to investigate its structure, morphology, and optical properties. The photocatalytic performance was evaluated through the degradation of Rhodamine B (RhB) under visible-light irradiation. The results showed that $(BiO)_2CO_3$@$ZnCo_2O_4$ achieved a degradation efficiency of 78.6%, which was about 2.6 times higher than that of pure $ZnCo_2O_4$ under the same conditions (120 min irradiation, catalyst dosage of 1.0 g/L, and initial RhB concentration of 30 ppm). This improvement is mainly attributed to the formation of a heterojunction, which enhances the separation of photogenerated charge carriers. When persulfate (PS, 0.25 g/L) was introduced, the degradation efficiency further increased to 98.9%, and the reaction rate was significantly enhanced (3.8 times higher than that without PS). This result suggests that the combination of photocatalysis and PS activation significantly improves degradation performance. Overall, the $(BiO)_2CO_3$@$ZnCo_2O_4$/PS system shows good potential for the removal of organic pollutants under visible light.

Keywords. heterojunction; $(BiO)_2CO_3$; $ZnCo_2O_4$;photocatalytic; persulfate**.**

1. INTRODUCTION

Rhodamine B (RhB) is the most commonly used organic dye in industry, particularly in textile dyeing techniques, due to its colour fastness, solubility, and affordability. However, RhB molecules released into aquatic ecosystems provide a significant risk to ecological integrity and human health. Consequently, it is essential to develop efficient techniques to eliminate RhB from dye effluent [1, 2]. In recent years, photocatalytic technology utilising semiconductors to convert solar energy into chemical energy for the rapid degradation of organic dye molecules has gained widespread use. Certain photocatalytic compounds have been effectively investigated, including TiO_2, ZnO, $(BiO)_2CO_3$; $ZnCo_2O_4$….[3]. The typical formula for spinel is AB_2O_4, where A is a divalent cation in the tetrahedral position (A) and a trivalent cation in the octahedral position (B). Spinel exhibits a multitude of unique features; particularly for spinel composed of transition metals, its most remarkable characteristic is its photocatalytic capability, such as $ZnCo_2O_4$, $CaFe_2O_4$, $CoFe_2O_4$…

$ZnCo_2O_4$ exhibits superior photoelectrochemical stability, enhanced electrical conductivity, and a higher density of redox-active sites compared to metal oxides (ZnO, Co_3O_4, etc.), which has attracted considerable research interest [4, 5]. Spinel $ZnCo_2O_4$, as a p-type semiconductor, is gaining prominence due to its many allotropic forms, non-toxicity, and affordability, making it applicable in several domains. In photocatalysis, spinel $ZnCo_2O_4$ is hindered by a limited energy band, resulting in the rapid recombination of photogenerated electrons and holes after light absorption. The construction of an effective heterojunction between $ZnCo_2O_4$ and other photocatalysts is thus proposed to enhance the photocatalytic performance of $ZnCo_2O_4$. Bismuth subcarbonate $(BiO)_2CO_3$ is a non-toxic, environmentally friendly photocatalyst consisting of alternating layers of $Bi_2O_2^{2+}$ and CO_3^{2-}[6, 7]. Nonetheless, $(BiO)_2CO_3$ has a high band gap energy (E_g = 3.0-3.3 eV), which restricts its excitation to ultraviolet light and limits its solar energy conversion efficiency [1, 7]. The goal of this work was to synthesise a heterojunction photocatalyst that can overcome the material's light-absorption limitations by integrating $(BiO)_2CO_3$ and $ZnCo_2O_4$ at different energy levels. The photocatalytic efficiency of the heterojunction $(BiO)_2CO_3$@$ZnCo_2O_4$ was evaluated in the presence of PS for the degradation of RhB under visible light.

© 2026 Trường Đại học Công nghiệp Thành phố Hồ Chí Minh

2. EXPERIMENTAL

2.1 Synthesis of $ZnCo_2O_4$

Gradually introduce 200 mL of $Zn(CH_3COO)_2$ 0.1 M solution and $Co(NO_3)_2$ 0.2 M in a molar ratio of Zn^{2+}/Co^{2+} = 1/2 into 100 mL of NaOH 0.5 M solution. The combination exhibits a pink precipitate, stabilises at pH 10, and is uniformly stirred throughout the process. Upon completion of the reaction, maintain stirring for an additional 60 minutes, then centrifuge and filter until the precipitate's washing water reaches pH 7. Dry the sample at 100°C for 4 hours, then heat it to 600°C at 5°C/min for 2 hours to obtain a black powder, designated ZC.

2.2 Synthesis of $(BiO)_2CO_3@ZnCo_2O_4$

The synthesis of $(BiO)_2CO_3@ZnCo_2O_4$ was carried out according to a modified co-precipitation method [8]. First, 0.57 g $Bi(NO_3)_3 \cdot 5H_2O$ and 100 mg citric acid ($C_6H_8O_7$) were dissolved in 30 mL of HNO_3 1.6 M to obtain solution A. Separately, 1 g Na_2CO_3 and 0.15 g cetyltrimethylammonium bromide (CTAB) were dissolved in 60 mL of deionised water under stirring for 30 min to form solution B. Subsequently, 2 g of the as-prepared ZC was dispersed into solution B, producing suspension B. Solution A was then slowly added dropwise into suspension B under continuous stirring. The reaction mixture was stirred for an additional 2 h at room temperature to ensure complete deposition. The resulting precipitate was collected by centrifugation, washed several times with ethanol, and dried at 60 °C, yielding a white composite powder, designated as BiC@ZC. For comparison, pure $(BiO)_2CO_3$ (BiC) was synthesised following the same procedure without the addition of ZC in suspension B.

2.3 Catalytic activity evaluation

The catalytic efficacy of the synthesised materials was evaluated by measuring the degradation of the RhB dye. The m(g) of the synthesised materials was incorporated into a catalytic system comprising two glass layers; the inner layer contained 100 mL of RhB dye solution at 30 ppm (C_{in}), while the outer layer provided a circulating water source to maintain stable temperatures. The system was consistently agitated throughout the two-step response.

Table 1. Photocatalytic degradation experiments of RhB under six different conditions (30ppm RhB)

System	Catalyst	PS (g/L)	catalyst dosage (g/L)	Light condition	Dark time (min)	Light time (min)
PS/Vis	0	0.25	0	Visible	60	120
BiC@ZC/PS	BiC@ZC	0.25	1	Dark	180	0
BiC/PS/Vis	BiC	0.25	1	Visible	60	120
ZC/PS/Vis	ZC	0.25	1	Visible	60	120
BiC@ZC/Vis	BiC@ZC	0	1	Visible	60	120
BiC@ZC/PS/Vis	BiC@ZC	0.25	1	Visible	60	120

Light off: Place the photocatalytic system in the dark to allow the substance to reach equilibrium/desorption. Thereafter, measure the RhB (Co) concentration.

Light on: Introduce 0.25 g/L PS activation into the system, then direct a halogen lamp (Osram 64640 HLX 150W, 24V, Germany) onto the photocatalytic system for 120 minutes. Evaluate the temporal variation in RhB concentration; every 30 minutes, remove 3 mL of the suspension, centrifuge, filter, and then quantify the RhB concentration (C_t). The concentration of RhB is ascertained using UV-Vis spectroscopy at a peak wavelength of 554 nm. Photocatalytic degradation experiments of RhB under six different conditions are shown in T**able 1**. The catalytic activity of the composite material was assessed by examining factors including the initial RhB concentration, catalyst loading, and PS activation loading. The examined variables were adjusted to their maximum levels, while all other variables remained constant.

3. RESULTS AND DISCUSSION

3.1 Characterization

Fig. 1A displays the X-ray diffraction patterns for the BiC, ZC, and BiC@ZC samples. The ZC sample exhibits diffraction peaks at 2θ values of 18.18°; 31.23°; 36.72°; 38.57°; 44.69°; 55.62°; 59.34° and 65.31, which are assigned to $ZnCo_2O_4$ (JCPDS No 23–1390) [9, 10]. The BiC shows diffraction peaks at 13.15°; 23.96°; 26.61°; 30.37°; 32.83°; 35.24°; 39.52°; 46.96°; 48.78°; 54.46°; 56.66° and 58.11° which can be assigned to $(BiO)_2CO_3$ (JCPDS No. 41-1488) [1, 11]. Upon loading BiC onto the ZC surface at a mass ratio of BiC/ZC of 10%, the X-ray diffraction pattern of the BiC@ZC sample shows that, besides the typical peaks of ZC, the intensity of these peaks decreases compared to pure ZC, while the characteristic peaks of BiC remain undetected. The cause may be the low BiC content relative to ZC; the interaction between BiC and ZC slightly weakens the ZC peaks in the BiC@ZC sample. The sharp peaks and the absence of additional peaks indicate that the synthesised samples are highly pure and contain few impurities.

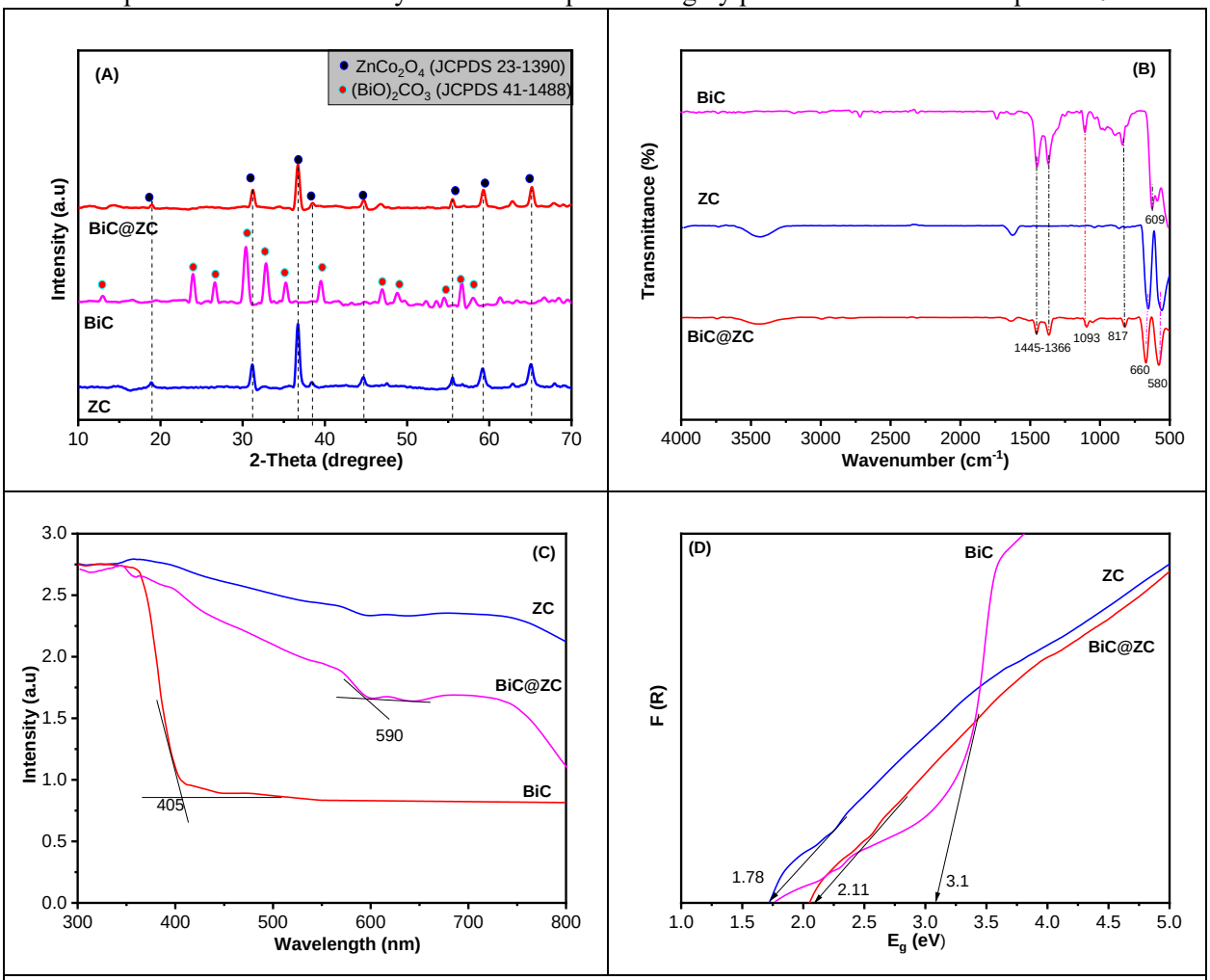


Fig. 1 (A) X-ray diffraction, (B) FT-IR, and (C, D) UV-vis DRS and E_g of BiC, ZC, and BiC@ZC samples.

Fig. 1B presents the FT-IR spectra used to identify the functional groups in the BiC, ZC, and BiC@ZC samples. The BiC sample shows characteristic peaks at 845 and 1398 cm^{-1}, attributed to the stretching vibrations of the CO_3^{2-} group, and a Bi–O–Bi stretching vibration is observed around 627 cm^{-1} [1, 11]. Strong absorption bands at 580 and 660 cm^{-1} belong to the metal–oxygen bonds corresponding to the Co–O and Zn–O stretching vibrations of the spinel structure of $ZnCo_2O_4$ [9, 10]. In addition to the characteristic vibrations of ZC, the BiC@ZC sample also displays CO_3^{2-} vibrations; however, the peak intensities have decreased. The X-ray diffraction and FT-IR results confirm the successful formation of the BiC@ZC heterostructure.

The optical properties of the synthesised materials, BiC, ZC, and BiC@ZC, were evaluated using UV-Vis DRS. **Fig. 1C** illustrates that BiC has an absorption edge at 405 nm, indicating its absorption mainly in the UV region [12]. ZC is black and absorbs light across the UV-visible spectrum, indicating strong

absorption. However, the band gap energy is small, which facilitates the recombination of photogenerated electron-hole pairs [13]. The combination of ZC and BiC results in BiC@ZC exhibiting an absorption edge at 590 nm, demonstrating a red shift relative to BiC and a blue shift relative to ZC. This result suggests that BiC@ZC exhibits an extended light absorption range, highlighting its potential for photocatalytic applications.

The SEM images revealed that ZC mainly consists of spherical particles with irregular size and shape, due to agglomeration, with particle sizes in the range of 15–40 nm (**Fig. 2A**). The BiC exhibited nanosheet-like structures with irregular **sizes** ranging from approximately 80 to 100 nm, characterised by rough surfaces and a relatively uniform distribution. Consequently, gaps are observed within the particle clusters, indicating that the adhesion among the particles was relatively weak (**Fig. 2B**). The SEM and TEM images (**Fig. 2C-D**) of the BiC@ZC sample indicated that BiC was larger than ZC, resulting in the absence of a continuous coating and its presence as a "decorative point" which help disperse the agglomerated ZC particles, thereby increasing the material's surface area. The increase in BET surface area from 18.1 to 28.8 $m^2\ g^{-1}$ after forming ZC@BiC further confirms more effective dispersion of ZC on the BiC support. This is in good agreement with the SEM images, which show a more uniform distribution of ZC particles and reduced aggregation in the composite. The significant size disparity between the two phases increases the density of the heterojunction interface, thereby promoting charge separation and transfer.

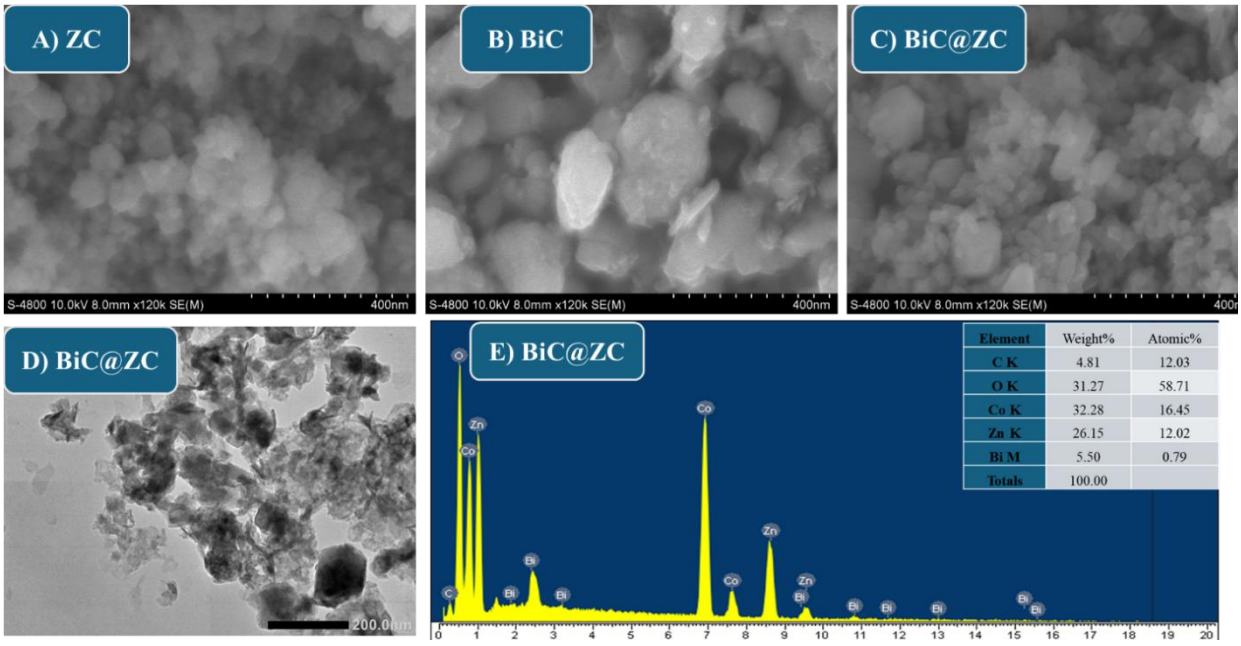


Fig. 2 SEM images of (A) BiC, (B) ZC, and (C) BiC@ZC samples. (D,E) TEM images and EDS of BiC@ZC samples.

The EDS spectrum **(Fig. 2E)** of BiC@ZC shows the presence of C, O, Co, Zn, and Bi, confirming the successful formation of the composite. The strong peaks of Co and Zn are attributed to $ZnCo_2O_4$, while Bi and C are from the $(BiO)_2CO_3$ component. The Bi content is relatively low (5.50 wt%), indicating that the amount of $(BiO)_2CO_3$ in the composite is small. This is consistent with the XRD results, which show that the characteristic peaks of $(BiO)_2CO_3$ are not clearly observed, likely due to its low content and good dispersion on the $ZnCo_2O_4$ surface

3.2 Degradation performance of the BiC@ZC system

The results of the investigation of the influence of different photocatalytic conditions (**Table 1**) on the synthesised materials are shown in **Fig. 3**. The pseudo-first-order Langmuir-Hinshelwood $\ln\frac{C_o}{C_t} = k_1.t$ .A kinetic model was used to assess the efficacy of the photocatalysts, as seen in **Fig. 3B.** The findings indicated that in PS/Vis conditions, the RhB degradation efficiency was relatively low, at 9.1%. This

demonstrated that RhB is difficult to degrade in the absence of a catalyst, whereas PS remains stable in the visible spectrum. In BiC@ZC/PS conditions, the RhB degradation efficiency was only 26.98%, with the adsorption process accounting for approximately 15% of RhB. This result also demonstrated that, in the absence of light irradiation, BiC@ZC shows negligible photocatalytic activity. The photocatalytic performances of ZC, BiC, and BiC@ZC were compared under identical conditions (PS = 0.25 g/L, RhB = 30 ppm, catalyst dosage = 1.0 g/L, dark adsorption time = 60 min, and irradiation time = 120 min). The results showed that BiC, ZC, and BiC@ZC can all adsorb RhB, with approximately 12-15% removal in 60 minutes in the dark. The RhB degradation efficiencies for BiC, ZC, and BiC@ZC were 38.92% ($k = 0.00863$ min^{-1}), 64.89 % ($k = 0.0034$ min^{-1}), and 98.97% ($k = 0.03304$ min^{-1}), respectively, in 120 minutes of light irradiation. The RhB degradation rate of BiC@ZC was approximately 3.8 times higher than that of ZC under identical conditions (**Fig. 3.C**).UV-vis DRS results indicate that ZC, with its dark colour, has a narrow band gap, leading to the formation of photogenerated electron-hole pairs upon light absorption, which then tend to recombine rapidly, consistent with typical photocatalytic behaviour. In contrast, BiC has a wide band gap, absorbing only UV light. Loading BiC onto the ZC surface results in a heterostructured composite, BiC@ZC. These two semiconductors interact to form a heterojunction, which facilitates charge transfer between photogenerated electrons and holes, reducing the recombination of photogenerated electron–hole pairs, extending the light absorption range, and increasing the RhB degradation efficiency of BiC@ZC [6, 10].

A comparison of the BiC@ZC heterojunction under two conditions: with PS activation (BiC@ZC/PS/Vis) and without PS (BiC@ZC/Vis). The findings indicate that applying the PS activation increased the degradation efficiency from 78.64% ($k = 0.0127$ min^{-1}) to 98.97% ($k = 0.03304$ min^{-1}), resulting in a 2.6-fold increase in the reaction rate. The possible explanation is as follows: in addition to the radicals capable of oxidising RhB, such as $O_2^{\bullet-}$, $OH^{\bullet}$, and photogenerated holes h^+ produced upon light absorption by the heterojunction, the PS activator, $S_2O_8^{2-}$ ions, can react with electrons to generate $SO_4^{\bullet-}$. Subsequently, $SO_4^{\bullet-}$ interacts with H_2O to produce $OH^{\bullet}$ free radicals that contribute to the degradation of RhB, as illustrated in Eqs (1) and (2) [14, 15]. The PS activation enhances the generation of reactive radicals, thereby reducing electron–hole recombination and increasing photocatalytic efficiency.

$$S_2O_8^{2-} + e^- \rightarrow SO_4^{\bullet-} + SO_4^{2-} \quad (1)$$

$$SO_4^{\bullet-} + H_2O \rightarrow SO_4^{2-} + {}^{\bullet}OH + H^+ \quad (2)$$

The study's experimental results on concentration variation with reaction time and the fitting to a pseudo-first-order kinetic model for RhB dye degradation using the synthesised materials showed that the equations had high correlation coefficients (R^2) ranging from 0.876 to 0.9566. Thus, the pseudo-first-order kinetic model can be used to describe the photocatalytic degradation process of RhB.

3.3 Effect of PS dosage

The PS can improve the reaction rate and enhance photocatalytic efficiency. In this study, the PS dosage varied from 0 to 0.4 g/L, whereas the BiC@ZC dosage (1.0 g/L) and RhB concentration (30 ppm) were kept constant. **Fig. 3D** illustrates the effect of PS dosage, showing that increasing PS dosage from 0 to 0.25 g/L led to a rapid increase in RhB degradation efficiency, from 78.64% to 98.97%. Increasing PS dosage enhanced ROS generation, as shown in Eqs. (1) and (2), thereby improving the degradation efficiency. As the PS dosage increased to 0.35 and 0.4 g/L, the RhB degradation efficiency declined slightly to 96.1%. The fixed amounts of BiC@ZC and incident light intensity led to an excess of $S_2O_8^{2-}$, which, according to Eqs (3) and (4), can scavenge $^{\bullet}OH$ and $SO_4^{\bullet-}$, resulting in a slight decrease in degradation efficiency [16, 17]

$$S_2O_8^{2-} + SO_4^{\bullet-} \rightarrow SO_4^{2-} + S_2O_8^{\bullet-} \quad (3)$$

$$S_2O_8^{2-} + {}^{\bullet}OH \rightarrow OH^- + S_2O_8^{\bullet-} \quad (4)$$

3.4 Effect of catalyst dosage

Fig. 3E shows the effects of catalyst dosage on RhB degradation efficiency as the BiC@ZC dosage was varied from 0.75 to 1.5 g/L. Increasing the loading from 0.75 to 1 g/L significantly enhanced RhB

degradation efficiency, rising from 89.57% to 98.97%, attributable to increased active sites and enhanced generation of reactive oxygen species (ROS). Nonetheless, when the BiC@ZC dosage reached 1.25–1.5 g/L, the RhB degradation efficiency decreased to 97.06% and 94.95%. Two reasons can explain this behaviour: i) The aggregation and sedimentation of catalyst particles reduce light penetration [18]. ii) As the BiC@ZC dosage increases, the number of active sites rises; nevertheless, the quantity of PS available is insufficient to react with the photogenerated electrons, resulting in a slight decrease in degradation efficiency [14]. The optimal dosage for subsequent experiments is 1.0 g/L.

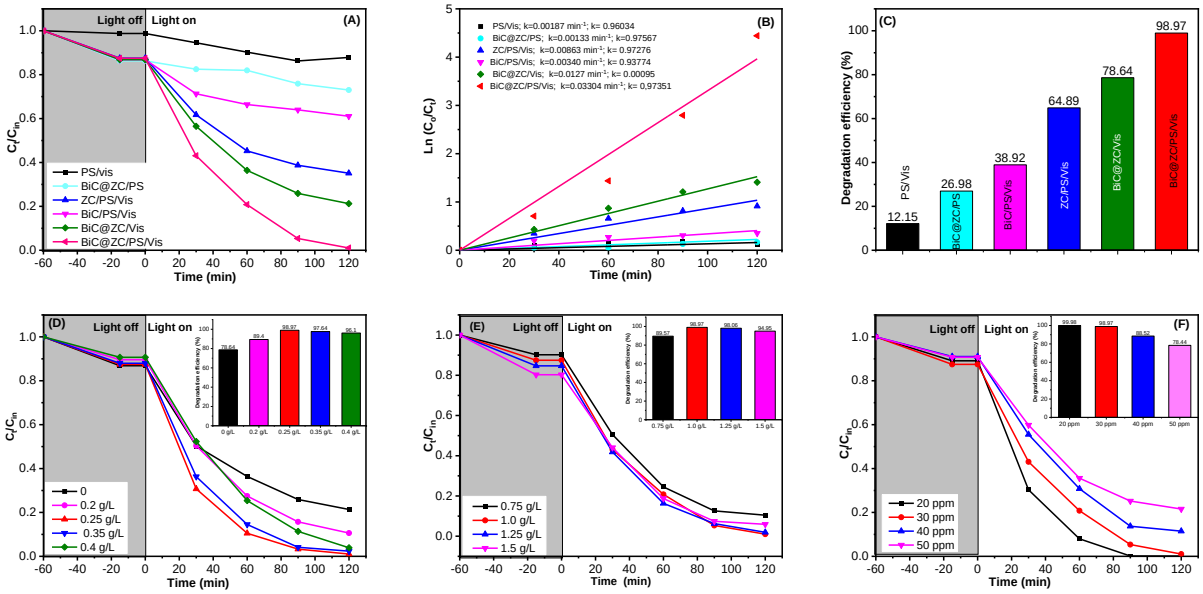


Fig. 3 (A) Effect of photocatalysts under different catalytic conditions on RhB degradation;(B) RhB degradation efficiency of the catalyst under different catalytic conditions; (C) first-order kinetic study of RhB degradation; (D) Effect of PS dosage; (E) Effect of catalyst dosage; (F) Effect of initial RhB concentration.

3.5 Effect of initial RhB concentration

The initial concentration of RhB is a crucial parameter for the photocatalytic process. The experiment was conducted with an initial RhB concentration of 20-50 ppm, a catalyst dosage of BiC@ZC of 1 g/L, a PS dosage of 0.25 g/L, and an irradiation time of 120 minutes. Fig. 3. F shows that increasing RhB concentration reduces the degradation efficiency of BiC@ZC. At a concentration of 20 ppm, the dye is almost completely degraded after 90 minutes of irradiation, whereas at 50 ppm, the degradation efficiency is 78.44% (**Fig. 3F)**. The light intensity of the simulated solar light source, catalyst dosage, and PS dosage were kept constant, resulting in a relatively constant ROS generation; hence, an increase in RhB concentration leads to a decrease in degradation efficiency. Moreover, an excessively high dye concentration may limit photon penetration, thus reducing the degradation efficiency [19].

3.6 Photocatalytic mechanism

Trapping experiments were conducted using *p*-BQ (as a scavenger for $O_2^{\bullet-}$), MeOH (for $SO_4^{\bullet-}$), EDTA (for h^+), and TBA (for $^{\bullet}OH$). These scavengers were introduced into the reaction system after reaching adsorption–desorption equilibrium in the dark. The results showed that the addition of MeOH led to the most significant decrease in RhB degradation efficiency (46.45%), followed by EDTA (63.58%). In contrast, the presence of BQ and TBA resulted in only slight reductions in degradation efficiency, to 74.05% and 85.43%, respectively (**Fig. 4A)**. These findings indicate that $SO_4^{\bullet-}$ is the dominant reactive species, with h^+ also playing an important role, while $O_2^{\bullet-}$ and $^{\bullet}OH$ contribute to a lesser extent.

The band gap energies of ZC and BiC, calculated from their maximum absorption wavelengths as seen in **Fig. 1D** using the Kubelka–Munk function, were estimated to be 1.78 eV and 3.1 eV, respectively. The conduction band (CB) and valence band (VB) positions were determined using the equations $E_{VB} = X - E_e + 0.5E_g$ and $E_{CB} = E_{VB} - E_g$, where X is the electronegativity of the semiconductor (6.54 eV for BiC and

4.94 eV for ZC), and E_e represents the energy of free electrons on the hydrogen standard scale (approximately 4.5 eV) [1, 10]. Accordingly, the CB and VB of ZC were calculated at – 0.45 eV and 1.33 eV, respectively, while those of BiC were 0.49 eV and 3.59 eV, respectively.

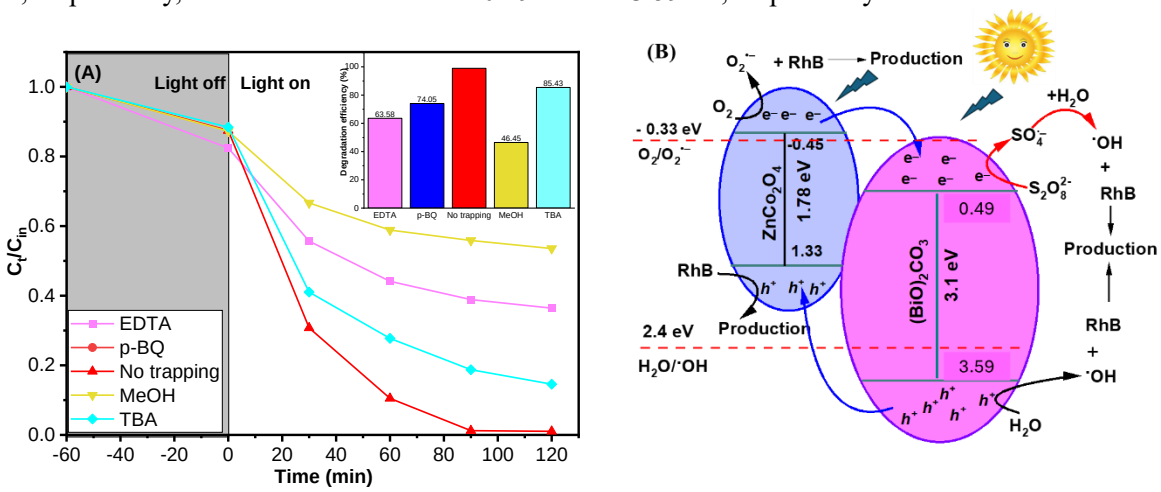


Fig.4 (A) Effects of radical scavengers on RhB degradation; (B) Schematic diagram of the mechanism of RhB decomposition of PS-activated BiC@ZC

Based on these results, a possible photocatalytic mechanism is proposed and illustrated in **Fig. 4B.** Under visible-light irradiation, both BiC and ZC are excited, generating electron–hole pairs. The CB position of ZC (E_{CB} = – 0.45 eV) is more negative than the $O_2/O_2^{\bullet-}$ reduction potential ($E°_{O2/O2\bullet-}$ = – 0.33 eV) [1], resulting in the electrons reacting with O_2 adsorbed on the material surface to generate $O_2^{\bullet-}$, which subsequently contributes to the degradation of RhB [1, 8]. These electrons may participate in interfacial electron transfer processes and contribute to the activation of $S_2O_8^{2-}$, as described in Eqs. (1) and (2), leading to the generation of reactive species such as $SO_4^{\bullet-}$, which further contribute to RhB degradation. In addition, the photogenerated holes in the VB of BiC (E_{VB} = 3.59 eV) may migrate to the VB of ZC (E_{VB} = 1.33 eV) due to the potential difference, where they can directly oxidise RhB. Furthermore, the photogenerated holes in the VB of BiC can react with H_2O ($E°_{\bullet OH/H2O}$ = 2.4 eV) to form $^{\bullet}OH$ [1, 13], which subsequently contributes to RhB degradation.

4. CONCLUSION

The $(BiO)_2CO_3$@$ZnCo_2O_4$ heterojunction was successfully synthesised. SEM analysis revealed that $(BiO)_2CO_3$ was unevenly distributed on the $ZnCo_2O_4$ surface, which may influence the photocatalytic performance of the composite. The results demonstrate that $BiO)_2CO_3$@$ZnCo_2O_4$ exhibits superior RhB degradation compared to pristine $(BiO)_2CO_3$ and $ZnCo_2O_4$ under visible-light irradiation. Under optimal conditions (60 min adsorption, 120 min irradiation, catalyst dosage of 1.0 g/L, and initial RhB concentration of 30 ppm), the degradation efficiency reached 78.64%. Notably, the efficiency was further enhanced to 98.9% upon the addition of PS (0.25 g/L) under identical conditions. The enhanced performance can be attributed to the synergistic effect between photocatalysis and persulfate activation. In this system, PS is activated by photogenerated electrons, producing $SO_4^{\bullet-}$, radicals, which serve as the dominant reactive species. These radicals can further react with H_2O to generate $^{\bullet}OH$, thereby contributing to the degradation of RhB.

ACKNOWLEDGEMENTS

This research is supported by the Industrial University of Ho Chi Minh City (IUH) under grant number 85/HĐ-ĐHCN; 22/12/2025 (25BCNHH05).

REFERENCES

1. Zhang, Q., Xie, F., Wang, J., Wang, T., Lei, J., Li, W., Cheng, J., Zhang, Y.: In-situ construction of $Bi_2O_2CO_3$/MIL-101(Cr) nanosheet catalyst for enhanced photocatalytic degradation of organic dye molecules from water. Appl. Organomet. Chem. 38, (2024). https://doi.org/10.1002/aoc.7614
2. Wang, B., Huang, L., Li, S., Qi, L.: Synthesis of Co_3O_4/BiOBr/BiOI Ternary Heterostructure and its Photocatalytic Degradation of RhB. Water Air Soil Pollut. 235, (2024). https://doi.org/10.1007/s11270-024-07192-4
3. Low, J., Yu, J., Jaroniec, M., Wageh, S., Al-Ghamdi, A.A.: Heterojunction Photocatalysts, 29,1601694 (2017). https://doi.org/10.1002/adma.201601694
4. Zhang, W., Xu, C., Liu, E., Fan, J., Hu, X.: Facile strategy to construction Z-scheme $ZnCo_2O_4$/g-C_3N_4 photocatalyst with efficient H_2 evolution activity. Appl. Surf. Sci. 515, (2020). https://doi.org/10.1016/j.apsusc.2020.146039
5. Li, X., Li, Y., Guo, X., Jin, Z.: Design and synthesis of $ZnCo_2O_4$/CdS for substantially improved photocatalytic hydrogen production. Front. Chem. Sci. Eng. 17, 606–616 (2023). https://doi.org/10.1007/s11705-022-2233-4
6. Si, Y., Li, J., Zhong, J., Zeng, J., Huang, S., Yuan, W., Li, M., Ding, J.: Charge separation properties of $(BiO)_2CO_3$/BiOI heterostructures with enhanced solar-driven photocatalytic activity. Current Applied Physics. 16, 240–244 (2016). https://doi.org/10.1016/j.cap.2015.12.008
7. Huang, S., Wu, Y., Zhang, Q., Jin, X., Li, D., Liu, H., Chen, P., Lv, W., Liu, G.: $Bi_2O_2CO_3$/Bi_2O_3 Z-scheme photocatalyst with oxygen vacancies and Bi for enhanced visible-light photocatalytic degradation of tetracycline. Environ. Sci. Nano. 9, 2104–2120 (2022). https://doi.org/10.1039/d1en01168e
8. Qin, Y.L., Wang, Y.Q., Zhao, P.Y., Liu, X.Y., Liu, Z.Y., Ni, D.R., Xiao, B.L., Ma, Z.Y.: Novel p–n junction photocatalyst of BiOCl/$(BiO)_2CO_3$ anchored on RGO with enhanced visible light photocatalytic activity. Appl. Phys. A Mater. Sci. Process. 126, (2020). https://doi.org/10.1007/s00339-020-04044-w
9. Priya, M., Premkumar, V.K., Vasantharani, P., Sivakumar, G.: Structural and electrochemical properties of $ZnCo_2O_4$ nanoparticles synthesized by hydrothermal method. Vacuum. 167, 307–312 (2019). https://doi.org/10.1016/j.vacuum.2019.06.020
10. Tan, B., Fang, Y., Chen, Q., Ao, X., Cao, Y.: Preparation of a $CaFe_2O_4$/$ZnCo_2O_4$ composite material and its photocatalytic degradation of tetracycline. Opt. Mater. (Amst). 109, (2020). https://doi.org/10.1016/j.optmat.2020.110470
11. Vahabirad, S., Nezamzadeh-Ejhieh, A., Mirmohammadi, M.: The coupled BiOI/$(BiO)_2CO_3$ catalyst: Brief characterization, and study of its photocatalytic kinetics. J. Solid State Chem. 314, (2022). https://doi.org/10.1016/j.jssc.2022.123405
12. Wang, F., Zhan, S., Zhou, F., He, Q., Zhang, C., Lai, J., Song, Y.: In-situ synthesis of BiO on 3D-3D-shaped $(BiO)_2CO_3$ surface for photocatalytic inactivation: Metal self-doping mechanism. J. Environ. Chem. Eng. 10, (2022). https://doi.org/10.1016/j.jece.2022.107576
13. Benhebal, H., Wolfs, C., Kadi, S., Tilkin, R.G., Allouche, B., Belabid, R., Collard, V., Felten, A., Louette, P., Lambert, S.D., Mahy, J.G.: Visible light sensitive SnO_2/$ZnCo_2O_4$ material for the photocatalytic removal of organic pollutants in water. Inorganics (Basel). 7, (2019). https://doi.org/10.3390/INORGANICS7060077
14. Liu, W., Zhou, J., Yao, J.: Shuttle-like CeO_2/g-C_3N_4 composite combined with persulfate for the enhanced photocatalytic degradation of norfloxacin under visible light. Ecotoxicol. Environ. Saf. 190, (2020). https://doi.org/10.1016/j.ecoenv.2019.110062
15. Tho, N.T.M., Tran Nguyen, M.A.: Construction of novel Bi_2S_3@Zn-Co-cLDHs heterojunction for enhanced photocatalytic degradation of levofloxacin with persulfate activation under visible light: mechanism and degradation pathway. RSC Adv. 15, 25839–25853 (2025). https://doi.org/10.1039/d5ra03086b
16. Lu, X., Wu, L., Liang, L., Liu, D., Chen, Y., Zeng, Y., Zhong, M., Jia, B.: Levofloxacin degradation by porous Cox/CN activated peroxymonosulfate: Investigation of efficiency, mechanism, and degradation pathways. Journal of Water Process Engineering. 56, (2023). https://doi.org/10.1016/j.jwpe.2023.104427.
17. Wang, Q., Wang, B., Ma, Y., Xing, S.: Enhanced superoxide radical production for ofloxacin removal via persulfate activation with Cu-Fe oxide. Chemical Engineering Journal. 354, 473–480 (2018). https://doi.org/10.1016/j.cej.2018.08.055
18. Rao, Y., Zhang, Y., Li, A., Zhang, T., Jiao, T.: Photocatalytic activity of G-TiO_2@Fe_3O_4 with persulfate for degradation of alizarin red S under visible light. Chemosphere. 266, (2021). https://doi.org/10.1016/j.chemosphere.2020.129236
19. Zhang, J., Zhang, S., Bian, X., Yin, Y., Huang, W., Liu, C., Liang, X., Li, F.: High Efficiency Removal Performance of Tetracycline by Magnetic $CoFe_2O_4$/$NaBiO_3$ Photocatalytic Synergistic Persulfate Technology. Molecules. 29, 4055 (2024). https://doi.org/10.3390/molecules29174055

HOẠT TÍNH QUANG XÚC TÁC CỦA $(BIO)_2CO_3@ZNCO_2O_4$ ĐƯỢC HOẠT HÓA BẰNG PERSULFAT PHÂN HỦY RHB DƯỚI ÁNH SÁNG NHÌN THẤY

NGUYỄN THỊ MAI THƠ*, NGUYỄN QUỐC THẮNG
Khoa Công nghệ Hóa học, Trường Đại học Công nghiệp TPHCM
** Tác giả liên hệ: nguyenthimaitho@iuh.edu.vn*

Tóm tắt. Trong nghiên cứu này, chất xúc tác quang $(BiO)_2CO_3@ZnCo_2O_4$, đã được tổng hợp thành công thông qua phương pháp đồng kết tủa đồng thời và nhiệt. Các tính chất lý hóa của vật liệu được đặc trưng một cách có hệ thống bằng các phân tích XRD, FT-IR, SEM, TEM và UV–Vis DRS để xác định thành phần pha, hình thái và khả năng hấp thụ quang học của nó. Hoạt tính xúc tác quang được đánh giá bằng cách đo sự phân hủy Rhodamine B (RhB) dưới bức xạ ánh sáng nhìn thấy. Kết quả cho thấy $(BiO)_2CO_3@ZnCo_2O_4$ đạt hiệu quả phân hủy RhB là 78,6%, với tốc độ phản ứng cao hơn 2,6 lần so với $ZnCo_2O_4$ sau 120 phút chiếu xạ (lượng chất xúc tác: 1,0 g/L; nồng độ RhB ban đầu: 30 ppm). Sự hình thành cấu trúc dị thể giữa $(BiO)_2CO_3$ và $ZnCo_2O_4$ tạo ra hiệu ứng hiệp đồng, tăng cường sự tách điện tích và do đó cải thiện hiệu quả quang xúc tác. Hơn nữa, khi có mặt persulfat (PS, 0,25 g/L), hiệu quả phân hủy RhB tăng lên 98,9%, và tốc độ phản ứng biểu kiến cao hơn 3,8 lần so với $(BiO)_2CO_3@ZnCo_2O_4$ không có PS. Những phát hiện này chứng minh rằng $(BiO)_2CO_3@ZnCo_2O_4$ được hoạt hóa bằng PS là chất quang xúc tác hiệu quả cao để loại bỏ RhB bằng ánh sáng nhìn thấy.

Received on January 20, 2026
Revised on April 10, 2026